Malaysian Journal of Chemistry, 2026, Vol. 28(1), 326-340
(Special Issue: *12th International Conference of the College of Science & 3rd Conference of Chemistry Department 2025*)

Hemolytic Impact of Green-Synthesized Gold and Silver Nanoparticles Using Plant Extracts with MDA as a Biomarker

Shahad Fadhel Ali[1,2]* and Wadhah Naji Jasim[1]
[1]University of Baghdad, College of Science, Department of Chemistry, Baghdad, Iraq
[2]Al-Nahrain University, College of Science, Department of Forensic Evidence, Baghdad, Iraq
Corresponding author (e-mail: shahad.ali2305@sc.uobaghdad.edu.iq)

The study investigates the green synthesis of gold and silver nanoparticles using Indian costus and Echinops spinosissimus extracts, focusing on their hemolytic and oxidative effects on red blood cells (RBCs). It aims to understand how nanoparticle concentration and exposure time influence membrane lipid peroxidation (MDA levels), providing insight into their biocompatibility and potential biomedical safety. The synthesis was optimized under standardized conditions, employing 0.02 M solutions of metal salts, 10 mL of *Echinops spinosissimus seeds* extract, and 6 mL of Indian installment. The optimal reaction proceeded at 70 °C for one hour with continuous stirring at neutral pH (7). The resulting nanoparticles exhibited a spherical morphology with sizes below 100 nm, as confirmed by scanning electron microscopy (SEM). The biological activity of the biosynthesized nanoparticles was evaluated through their impact on human red blood cells (RBCs). Hemolysis was assessed by measuring malondialdehyde (MDA) as a marker of oxidative membrane damage and compared with chemically synthesized nanoparticles of 50 nm. The results revealed RBC lysis induced by both silver and gold nanoparticles, with variations in hemolytic intensity influenced by the type of metal and the plant extract employed in green synthesis.

Keywords: Green Synthesis, nanoparticles, Indian installment, Echinops spinosissimus, Hemolysis, SEM

Received: September 2025; Accepted: October 2025

In recent years, nanotechnology has emerged as one of the most promising fields in science and engineering due to its diverse applications in medicine, agriculture, catalysis, and environmental protection. Among metallic nanoparticles, silver (AgNPs) and gold nanoparticles (AuNPs) have attracted particular attention because of their distinctive physicochemical properties [1]. AgNPs are well recognized for their potent antimicrobial activity, catalytic potential, and surface plasmon resonance behavior, while AuNPs are valued for their chemical stability, biocompatibility, and optical properties that make them useful in diagnostics, drug delivery, and photothermal therapies. Conventional wet-chemical routes for producing both AgNPs and AuNPs often require strong reducing agents and synthetic stabilizers, which may generate hazardous residues, lead to high solvent waste, and increase the risk of metal ion leaching, raising concerns regarding environmental and biological safety [2]. To overcome these limitations, green nanochemistry has advanced plant-extract–mediated synthesis of AgNPs and AuNPs, operating in aqueous systems under mild conditions. In such approaches, endogenous phytochemicals serve dual roles: reducing metal ions ($Ag^{+} \rightarrow Ag^{0}$, $Au^{3+} \rightarrow Au^{0}$) and stabilizing the resulting nanoparticles through surface capping. This process mitigates the need for toxic chemicals, reduces environmental burden, and enhances biocompatibility [3]. Hydroxyl, carbonyl, and carboxylate groups present in polyphenols, flavonoids, terpenoids, and organic acids donate electrons to metal ions, initiating rapid nucleation. While the same functional groups anchor to particle surfaces, forming durable capping layers that prevent uncontrolled aggregation and suppress ion leaching. Within this framework, *Indian installment* and *Echinops spinosissimus seeds* represent promising biogenic platforms for the green fabrication of both AgNPs and AuNPs. Indian installment, traditionally used in ethnomedicine, is rich in polyphenolic and redox-active metabolites that promote fast reduction of metal ions and simultaneously generate an organic corona that enhances nanoparticle stability [3]. This phytochemical capping is expected to limit the release of free silver or gold ions into the surrounding media, thereby improving safety and reducing leaching risks. Similarly, camel thorn, a desert shrub with abundant flavonoids, phenolics, and low–molecular–weight carbohydrates, provides natural reducing and chelating agents capable of not only converting Ag^{+} and Au^{3+} ions into metallic nanoparticles but also adsorbing strongly onto their surfaces to improve colloidal stability under physiological and environmental conditions. In the present work, aqueous extracts of Indian installment and Echinops spinosissimus seeds are employed as sole reducing and capping agents for the synthesis of both AgNPs and AuNPs. By

†Paper presented at the 12th International Conference of the College of Science & 3rd Conference of Chemistry Dept. 2025

optimizing extract concentration, pH, and temperature, it is possible to obtain nanoparticles with controlled size distributions, desirable morphologies, and enhanced stability [4]. Characterization techniques—including UV–visible spectroscopy to monitor surface plasmon resonance, FTIR to identify phytochemical capping groups, electron microscopy to determine particle size and morphology, zeta potential analysis to assess colloidal stability, and ICP-based assays to quantify metal ion release—were applied to establish structure–function relationships. Collectively, these results aim to demonstrate that plant-mediated AgNPs and AuNPs derived from Indian installment and Echinops spinosissimus seeds can be produced via eco-friendly, low-impact routes that minimize metal ion leaching while maintaining high functional performance, thereby aligning with the principles of sustainable nanotechnology [5].

Gold nanoparticles, emphasizing eco-friendly, low-toxic routes of nanoparticle production. For example, Fahim et al. (2024) reviewed advances in green synthesis of AgNPs, discussing how plant phytochemicals control particle size, stability, and biological compatibility [6]. Rónavári et al. (2021) compiled methods and characterization of green AgNPs and AuNPs, highlighting their biomedical potential and challenges in translating them safely in vivo. (7) Yang et al. (2024) reported new protocols for synthesizing AuNPs via Nicotiana leaf extract and assessed their stability and cytotoxicity under physiological conditions [8].

Parallel to synthesis innovations, many studies have examined nanoparticle-induced oxidative stress and hemolysis in red blood cells (RBCs). A landmark study by Pan et al. (2016) developed high-throughput in vitro assays to evaluate RBC sensitivity under oxidative, osmotic, and mechanical stresses when loaded with nanocarriers. [9] The work by Sing et al., "Nanotoxicity of Silver Nanoparticles to Red Blood Cells," established that AgNPs induce dose- and size-dependent hemolysis and reactive oxygen species generation in RBCs. [10] More broadly, Min et al. (2023) surveyed the molecular mechanisms by which metal-based nanoparticles generate ROS, trigger oxidative damage, inflammation, and cytotoxic effects with emphasis on how surface chemistry, size, and dissolution govern toxicity [11].

Other studies focused on balancing nanoparticle functionality with biocompatibility. Pinilla-Torres et al. (2023) synthesized AuNPs using mesquite gum and evaluated their hemocompatibility, showing negligible hemolysis over exposure times and concentrations. [12] Niżnik et al. (2024) provided a comprehensive review of AuNPs in biomedical fields, discussing toxicology, surface modifications, and safe dosage windows. [13] Finally, Liaqat et al. (2022) optimized green AgNPs synthesis and reported minimal cytotoxicity in mammalian cells at effective antimicrobial doses [14].

Effect of Silver and Gold Nanoparticles on Red Blood Cell Hemolysis

Silver nanoparticles (AgNPs) and gold nanoparticles (AuNPs) have attracted significant interest due to their unique physicochemical and biomedical properties, yet their interactions with mammalian cells raise critical questions about hemocompatibility [15]. Red blood cells (RBCs), being the most abundant cellular component of blood, serve as an important model to evaluate the potential hemolytic effects of these nanomaterials. When either AgNPs or AuNPs come into direct contact with the erythrocyte membrane, they may induce structural and biochemical alterations that can culminate in hemolysis [16]. The erythrocyte membrane consists of a lipid bilayer enriched with phospholipids, cholesterol, and membrane proteins essential for maintaining osmotic balance and cellular integrity. AgNPs, particularly at smaller sizes (<20 nm), exhibit high surface reactivity that promotes direct adsorption onto the RBC surface, disrupting lipid packing and protein stability, which may increase membrane permeability. AuNPs, while also capable of interacting with the membrane, generally display lower catalytic reactivity, leading to less pronounced membrane perturbations. Oxidative stress represents a key mechanism underlying nanoparticle-induced hemolysis. AgNPs are well known for generating reactive oxygen species (ROS) either through surface reactions or by releasing silver ions (Ag^+), resulting in lipid peroxidation, protein oxidation, and cytoskeletal destabilization [17]. This cascade reduces membrane elasticity and promotes lysis under stress conditions. AuNPs, by contrast, are chemically more stable and less prone to ion release, thus producing a weaker oxidative response. Nonetheless, at higher concentrations or under prolonged exposure, even AuNPs can trigger measurable oxidative stress and contribute to hemolytic events [18].

Several factors modulate the extent of RBC disruption, including nanoparticle size, concentration, exposure time, and surface chemistry. Green-synthesized nanoparticles from plant extracts often retain natural phytochemical capping agents that improve stability, reduce ion release, and mitigate oxidative stress, thereby enhancing biocompatibility [19]. Still, dose dependence remains critical: at low to moderate concentrations, both AgNPs and AuNPs may exhibit minimal hemolysis, while high concentrations or poorly stabilized formulations markedly increase the risk of RBC lysis. Overall, both silver and gold nanoparticles can interact with red blood cells, but silver demonstrates a stronger hemolytic effect due to its higher oxidative potential, whereas gold shows comparatively milder interactions and better compatibility [20].

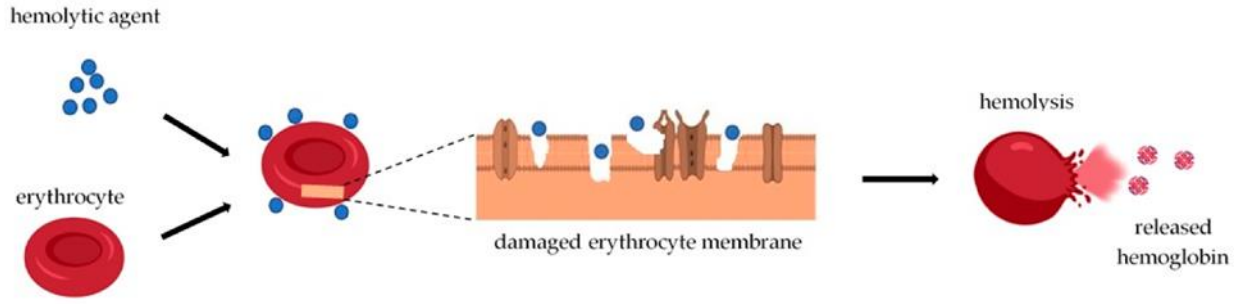

Figure 1. Schematic representation of the hemolysis process.

Inferring RBC Hemolysis from MDA after AgNP Exposure

Old nanoparticles (AuNPs) and silver nanoparticles (AgNPs) are widely studied for their biomedical potential, yet their interactions with red blood cells (RBCs) remain a critical determinant of hemocompatibility. Because RBCs lack nuclei and mitochondria, their viability depends largely on the structural stability of the plasma membrane. Disruption of the lipid bilayer by nanoparticles can initiate oxidative damage that culminates in hemolysis. A key marker of this process is malondialdehyde (MDA), a stable byproduct of lipid peroxidation [21]. The erythrocyte membrane is highly enriched in polyunsaturated fatty acids, making it particularly susceptible to oxidative attack. Interaction with AgNPs or AuNPs can disturb membrane integrity and trigger lipid oxidation, leading to the accumulation of MDA. Elevated MDA concentrations therefore, serve as a reliable indicator of membrane injury and early hemolytic potential. Comparative observations suggest that AgNPs, due to their higher redox reactivity and partial ion release, produce stronger increases in MDA levels than AuNPs [22]. In contrast, AuNPs typically induce milder changes, reflecting their relative chemical stability and reduced tendency to promote lipid peroxidation. Thus, monitoring MDA levels provides mechanistic insight into the degree of nanoparticle-induced oxidative stress on erythrocytes. The rise in MDA directly reflects lipid bilayer destabilization and precedes the overt rupture of RBCs, offering a sensitive method to evaluate the hemolytic effects of both silver and gold [23].

RESEARCH METHODOLOGY

Study Design and Overall Approach

This work adopts an experimental, comparative methodology grounded in green nanotechnology. Silver (AgNPs) and gold nanoparticles (AuNPs) are biosynthesized using aqueous plant extracts as dual reducing and capping agents, then physicochemically characterized and biologically evaluated on human red blood cells (RBCs). Hemolytic effects are quantified indirectly via lipid-peroxidation biomarker malondialdehyde (MDA) and directly via hemoglobin release, across graded nanoparticle: RBC ratios and timepoints to capture concentration- and time-dependent responses.

Materials: Characteristics, Rationale of the Study, and Applications

Plant extracts: (Indian installment “Indian costs” & Echinops spinosissimus “camel thorn”): Rich in polyphenols, flavonoids, and organic acids that donate electrons to Ag^{+}/Au^{3+} (reduction to Ag^{0}/Au^{0}) and adsorb onto surfaces to stabilize nascent nanoparticles. Chosen to enable eco-friendly synthesis, minimize ion leaching, and enhance biocompatibility in downstream blood assays.

Metal precursors: $AgNO_3$ and $HAuCl_4 \cdot 3H_2O$ are water-soluble salts that yield metallic NPs under mild conditions.

Biological matrix: Human RBCs provide a sensitive, nucleus-free model to assess hemocompatibility; their PUFA-rich membranes are susceptible to oxidative damage, making them suitable for MDA-based peroxidation readouts.

Buffers and media: Phosphate-buffered saline (PBS, pH 7.4) ensures physiological osmolarity and ionic strength, preserving RBC integrity during exposure.

Controls: A negative control (RBCs in PBS without NPs) establishes basal MDA/hemolysis; a positive control with synthetic nanoparticles (defined size) anchors comparative toxicity.

Instruments

UV–Visible spectrophotometer (200–800 nm range):

Readout: Surface plasmon resonance (SPR) bands characteristic of AgNPs/AuNPs; hemoglobin absorbance at ~540 nm for direct hemolysis quantification.

Purpose: Confirm nanoparticle formation and quantify RBC hemolysis from supernatants.

Scanning Electron Microscopy (SEM):

Readout: Morphology, primary particle size, dispersion/agglomeration state of AgNPs/AuNPs.

Purpose: Correlate shape/size with optical and hemolytic behavior; verify sub-100-nm spherical/ near-spherical products.

Atomic Force Microscopy (AFM):

Readout: Height maps, mean particle size distribution, and surface roughness parameters (e.g., Sa, Sq).

Purpose: Complement SEM with Nano topography and quantitative roughness that can influence RBC interactions.

Methods

Preparation of Solutions

Collection of Indian installments and Echinops spinosissimus: The plants were purchased from a herbal shop, ground finely, and then used as a reducing agent in the preparation of nanoparticles.

Preparation of Aqueous Extract of Indian Installment and Echinops Spinosissimus

The dried plant powder is weighed 5 grams and soaked in 100 ml of distilled water overnight, then boiled at 70 degrees Celsius for an hour, then filtered using filter paper and placed in a centrifuge at 5000 revolutions for 5 minutes [24].

Preparation of Silver Nitrate

Prepare a 0.1, 0.01, and 0.001 M silver nitrate stock solution by dissolving 3.39 g, 0.03 g, and 0.34 g of silver nitrate, respectively, in 200 mL of distilled water. Then, stored the stock solutions in the dark until they used them [25].

Preparation of Gold Salts Solution

Prepare a 0.01 M Gold salt stock solution by dissolving 3.393 g of HAuCl4.3H2O in 100 mL of distilled water. Then, the stock solutions were stored until used [26].

Optimized Conditions for Green Synthesis of AgNPs and AuNPs

This section examines the effects of several parameters, including extract, AgNO3, HAuCl4 concentrations, temperature, pH, and incubation period.

Plant Extract and $AgNO_3$, $HAuCl_4$ Concentrations

You can increase the concentration of plant extract in the reaction solution to enhance the absorbance intensity for both silver and gold nanoparticles. In practice, different milliliter volumes of plant extract (2 to 10 ml) are combined with either silver nitrate ($AgNO_3$) or chloroauric acid ($HAuCl_4$) solutions. At higher concentrations of plant extract, biomolecules act as efficient reducing and stabilizing agents, coating the nanoparticle surfaces, preventing aggregation, and thereby improving colloidal stability [27]. The concentration of the metal precursor plays a critical role in the green synthesis process. For $AgNO_3$, increasing its concentration can enhance absorbance intensity and lead to the formation of larger AgNPs, while for $HAuCl_4$, higher precursor concentrations similarly promote increased absorption and can influence the size, morphology, and uniformity of AuNPs. Thus, optimizing both plant extract and precursor concentrations is essential for controlling the physicochemical characteristics of biosynthesized silver and gold nanoparticles [28].

Incubation Period

The incubation period is another important factor influencing the size, stability, and yield of both silver (AgNPs) and gold nanoparticles (AuNPs). Prolonged incubation promotes the continued reduction of metal ions, leading to the generation of a greater number of nanoparticles and an increase in absorption intensity. During the synthesis of AgNPs, the reaction mixture gradually changes color from yellow to brown, whereas in the case of AuNPs, the solution shifts from pale yellow to ruby red or purple, confirming nanoparticle formation. These colorimetric transitions are characteristic indicators of successful biosynthesis and are directly associated with the surface plasmon resonance of the produced nanostructures [29].

Temperature

Temperature is one of the key variables influencing the shape and size of biosynthesized silver (AgNPs) and gold nanoparticles (AuNPs). Several studies have demonstrated that both AgNPs and AuNPs undergo morphological changes and show a decrease in particle size as the reaction temperature increases. Elevated temperatures accelerate the reduction of Ag^+ and Au^{3+} ions, promoting rapid nucleation and leading to the formation of numerous small, predominantly spherical nanoparticles [30]. Thus, temperature control is critical for tailoring the size distribution, morphology, and uniformity of both silver and gold nanostructures during green synthesis.

pH

In order to control the shape, size, and stability of silver (AgNPs) and gold nanoparticles (AuNPs),

previous studies have investigated the effect of altering the pH level during the synthesis process. The results indicated that a neutral pH range around 7 is optimal for ensuring the effective reduction of both Ag^{+} to Ag^{0} and Au^{3+} to Au^{0}, leading to higher yields of stable nanoparticles. Under these conditions, the biosynthesis process favors the formation of uniformly distributed particles, while extreme acidic or alkaline environments often result in irregular morphologies or reduced stability [31].

Phosphate Puffer Saline

Phosphate-buffered saline (PBS) is a buffer solution commonly used in biological research. The buffer helps to maintain a constant PH. The osmolarity and ion concentrations of the solutions match those of the human body (isotonic) [32]. The required compounds and their concentrations are listed in Table 1.

Procedure

1. Prepare 800 ml of distilled water in a suitable container.
2. Add 8g of NaCl to the solution.
3. Add 200 mg of KCl to the solution.
4. Add 1.44g of Na2HPO4 to the solution.
5. Add 245 mg of KH2PO4 to the solution.
6. Adjust the solution to the desired PH (typically PH=7.4).
7. Add distilled water until the volume is 1 L.

Collection of Blood Specimens

Peripheral blood samples were obtained from healthy volunteer donors aged 33 years, female, with no history of diabetes or other chronic illnesses. All participants were medication-free and had not received anticoagulants, antiplatelet agents, antibiotics, herbal preparations, or vitamin/mineral supplements for at least 14 days before donation [33]. Approximately 8 mL of venous blood was collected from each donor into sterile sodium citrate tubes to prevent coagulation and was processed immediately for subsequent experiments.

Preparation of 5% Red Blood Cell Suspension

Following blood collection and separation, the erythrocyte pellet obtained after repeated washing with phosphate-buffered saline (PBS, pH 7.4) was used to prepare a working suspension. A 5% (v/v) RBC suspension was prepared by diluting 0.5 mL of packed erythrocytes with PBS to a final volume of 10 mL. The suspension was gently mixed to avoid mechanical damage to the cells and was used immediately for hemolysis assays [34].

Hemolysis Assay

Standard hemolysis experiments were used to see how the nanoparticle surface chemistry affected human red blood cells (RBCs). It utilized red blood cells from preserved human blood sourced from Yarmouk Teaching Hospital. To keep the blood from clotting, 8 mL of blood was added to 0.8 mL of a 3.8% sodium citrate solution in a 10 mL Falcon tube. The blood was gently mixed and spun in a centrifuge at 5,000 RPM for 5 minutes [35]. We threw away the supernatant and washed the RBCs five times by putting them in a phosphate buffer saline solution with a pH of 7.4. The final suspension for the hemolysis assay was made up of 5% (v/v) RBCs in a phosphate buffer solution. To assess the hemolytic impact, varying concentrations of nanoparticles (20%, 50%, 80%) were incubated with red blood cells (200 µL of a 5% solution). The tubes were left at room temperature for 30, 60, and 90 minutes after being gently homogenized. In all of the studies, the hemolysis assay's final volume was 1.0 mL. After the incubation, the tubes were spun for 5 minutes, and then 100 µL were carefully taken from each tube and put on a clean 96-well plate. We measured the amount of hemoglobin in the supernatant of a nanoparticle-RBC mixture by measuring how much light it absorbed at 540 nm (Shimadzu, Kyoto, Japan). The positive control comprised 0.8 mL of deionized water and 0.2 mL of a 5% RBC suspension containing synthetic nanoparticles [36]. The negative control was made out of 0.8 mL of a phosphate buffer solution and 0.2 mL of the RBC suspension (5%).

Table 1. Phosphate buffer saline.

Compounds	The Weight	Concentration
Na2HPO4(Mw:141.96 g/mol)	1.44 g	0.01 M
NaCl (Mw: 58.4 g/mol)	8 g	0.137 M
KCl (Mw: 74.551 g/mol)	200 mg	0.0027 M
KH2PO4(Mw:136.086 g/mol)	245 mg	0.0018 M

RESULTS AND DISCUSSION

Characterization of Nanoparticles

Scanning Electron Microscopy (SEM) Imaging of Silver and Gold Nanoparticles:

The physicochemical properties of nanoparticles are important for their behavior, bio-distribution, safety, and efficacy. Based on the experimental findings, the optimal conditions for synthesizing silver nanoparticles were achieved using 10 mL of *Echinops spinosissimus* extract, while 6 mL of *Indian installment* extract proved suitable for the same purpose. The synthesis process required an integration time of 1 hour at a reaction temperature of 70 °C, with the pH maintained at a neutral value of 7. Gold nanoparticles were successfully synthesized under the same experimental conditions. Therefore, characterization of AgNPs is essential to evaluate the functional aspects of the synthesized particles. Scanning electron microscopy (SEM) is commonly employed to determine the morphology, size, and distribution of nanoparticles, providing valuable insights into their structural features [37]. The morphology of silver nanoparticles synthesized using *Indian installation and Echinops spinosissimus* extracts was examined by scanning electron microscopy (SEM). As shown in Figure 2. a, AgNPs produced by the *Indian installation* displayed predominantly spherical shapes with relatively small particle sizes ranging from ~19.4 to 23.4 nm. The nanoparticles were well dispersed, although occasional agglomerations were observed, likely due to partial clustering during the biosynthesis process. In contrast, Figure 2.b) illustrates AgNPs synthesized with *Echinops spinosissimus*, which exhibited larger particle sizes in the range of ~47.9 to 71.9 nm, with more frequent aggregation compared to those synthesized with *Indian installment*. The broader size distribution and clustering suggest differences in the phytochemical composition of the two plant extracts, which may influence the reduction rate of silver ions and the stability of the formed nanoparticles.

As shown in Figure 2.a, AuNPs produced with Indian installment extract exhibited relatively small particle sizes ranging between ~18.5 and 34.3 nm, with a generally spherical morphology and good dispersion, although some minor agglomerations were present.

In contrast, Figure 2.b shows AuNPs synthesized with *Echinops spinosissimus*, which revealed larger particle aggregates with less uniform distribution. The particles exhibited spherical to irregular morphologies and tended to form clusters, suggesting weaker stabilization compared with *Indian installment*-derived AuNPs. These findings indicate that while both plant extracts are effective in reducing Au^{3+} to Au^{0}, *Indian installment* extract produces smaller and more homogeneously dispersed AuNPs, whereas *Echinops spinosissimus* extract yields larger and more aggregated particles, likely due to differences in the phytochemical composition of the reducing and capping agents.

Atomic Force Microscopy (AFM)

We used the atomic force microscope to investigate the morphology of the surface, mean particle size distribution, root mean square height (Sq), and surface roughness (Sa), which we calculated using SPIP Mountains software. The two- and three-dimensional images (represented in Figure 4) show that the AgNPs in the 2D image appear spherical with a uniform distribution in the scanned area (3.58 x 3.58 m). Figure 5 shows that the mean diameter of 194 particles in the desired area is 63.55 nm. We scanned the samples using the tapping mode, determining surface roughness by changing the height and representing it with parameters Sa (3.489 nm) and Sq (4.392).

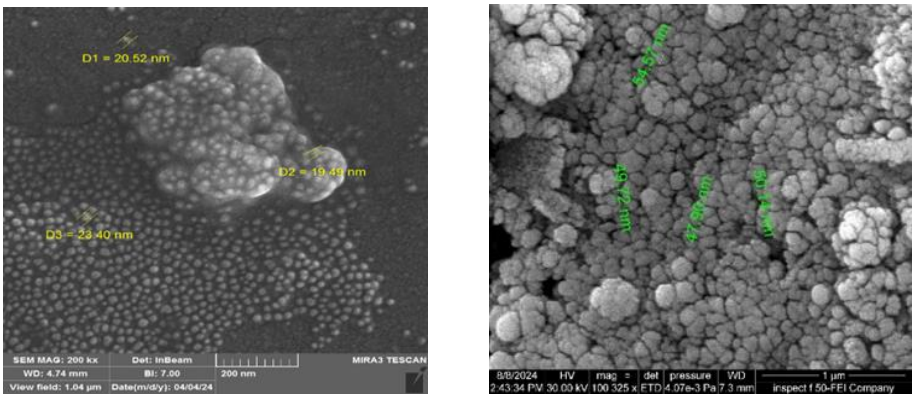

(a) (b)

Figure 2. Representative SEM micrographs of silver nanoparticles (AuNPs) synthesized using (a) *Indian installment* (b) *Echinops spinosissimus* plant extracts.

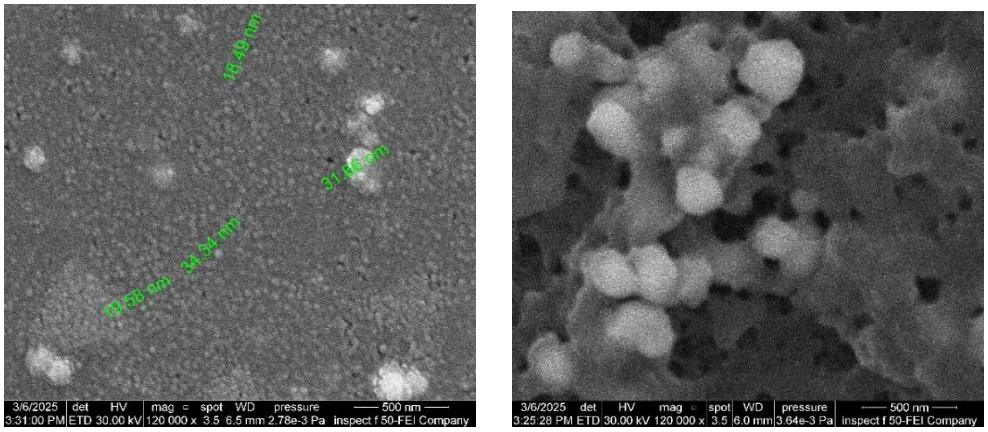

(a) (b)

Figure 3. Representative SEM micrographs of gold nanoparticles (AuNPs) synthesized using (a) Indian installment (b) Echinops spinosissimus plant extracts.

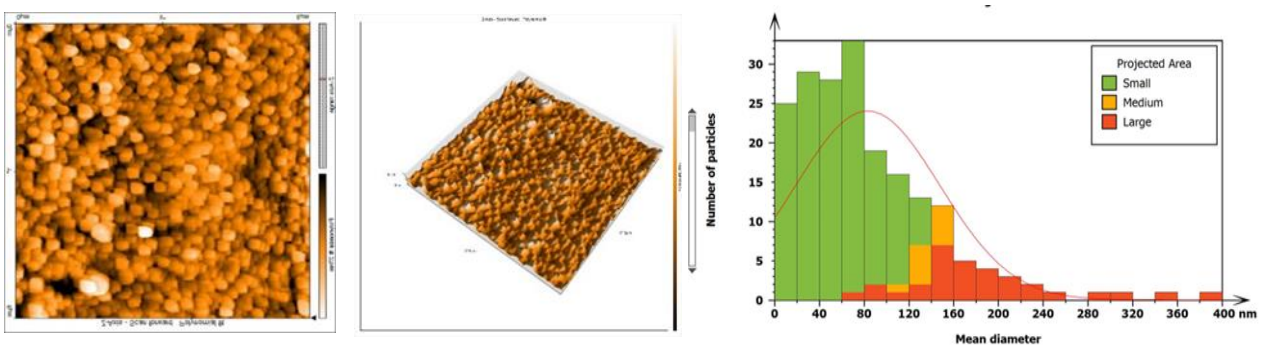

Figure 4. shows an AFM pictures of AgNPs nanoparticles made by green methods and the Distribution of diameter ranges of nanoparticles.

Table 2. Experimental groups included in the study.

Group	Description
G1	AuNPs synthesized with *Echinops spinosissimus* extract
G2	AgNPs synthesized with *Echinops spinosissimus* extract
G3	AuNPs synthesized with *Indian installments* extract
G4	AgNPs synthesized with *Indian installments* extract
G5	Positive control (synthetic AgNPs with volume 50 nm)
G6	Negative control (RBC without nanoparticles)

Malondialdehyde (MDA) as a Biomarker of Nanoparticle-Induced Hemolysis

Effect of concentrations on RBC Hemolysis (MDA levels)

Malondialdehyde (MDA) is a stable end-product of lipid peroxidation and a well-established biomarker for oxidative injury to red blood cell (RBC) membranes. When RBCs are exposed to silver nanoparticles (AgNPs) or gold nanoparticles (AuNPs), oxidative stress can lead to peroxidation of membrane lipids and subsequent hemolysis. AgNPs, due to their higher redox activity and partial release of Ag^+ ions, typically cause greater increases in MDA compared to AuNPs, which are more chemically stable and induce milder effects [38]. Measuring MDA levels thus provides a sensitive and mechanistic means to evaluate the hemolytic potential.

Table 3. Malondialdehyde (MDA) concentrations (nmol/ml) in erythrocytes of the tested groups (G1–G6) under different treatment conditions (ZERO, 80RBC20M, 50RBC50M, 20RBC80M), with corresponding Chi-square (X^2) and P values.

MDA Con. Nmol/ml 0.2-60	Tested groups						X^2 P value
	G1	G2	G3	G4	G5	G6	
ZERO	3.421	2.811	3.439	3.506	3.173	3.342	0.78 non sig
80RBC20M	3.517	3.985	3.369	3.503	4.022	3.884	0.32 non sig
50RBC50M	**1.446**	3.838	2.195	2.936	3.114	3.871	0.02 sig
20RBC80M	**7.951**	5.876	4.387	5.044	**6.214**	3.464	0.001 sig
X^2 P value	**0.02 sig**	**0.02 sig**	0.06 non sig	0.06 non sig	0.02 sig	0.91 non sig	

***. P-value is significant at the P≤ 0.05 level**

Experimental Groups

This study investigated the effects of gold and silver nanoparticles, synthesized via green methods using *Indian installment* and Echinops spinosissimus seeds, on red blood cells. The table presents the induction of lipid peroxidation in erythrocytes by these nanoparticles, as assessed through malondialdehyde (MDA) levels. Statistical analysis using the Chi-square test demonstrated that the hemolytic response of red blood cells is concentration-dependent and is significantly influenced by both the type of metallic nanoparticle and the plant extract employed in their synthesis. At baseline (zero concentration) and at the lowest exposure level, corresponding to 80% red blood cells and 20% nanoparticles, no statistically significant differences were observed among the tested groups. This indicates that at low nanoparticle concentrations, irrespective of the plant extract used in the synthesis, no substantial oxidative stress was induced, and hemolysis of red blood cells did not occur to a noticeable extent. These findings are consistent with previous studies on nanoparticle toxicity, which suggest that at sub-toxic concentrations, nanoparticles may exhibit relative biocompatibility with erythrocytes. At the intermediate concentration (50 red blood cells to 50 nanoparticles), statistically significant differences were observed, with a P-value of 0.02. Notably, Group 1 (gold nanoparticles synthesized using Echinops spinosissimus seeds) exhibited markedly lower levels of malondialdehyde compared to the other groups, suggesting a potential antioxidant or protective effect at this concentration. In contrast, the remaining groups displayed higher MDA levels, reflecting the complexity of nanoparticle interactions with red blood cells. This outcome indicates that the bioactive constituents of the plant extracts employed in the synthesis may differentially influence the biological activity of the nanoparticles against erythrocytes. At the highest nanoparticle concentration (20 red blood cells to 80 nanoparticles), highly significant differences were detected, with a P-value of 0.001. Silver nanoparticles synthesized using Echinops spinosissimus seeds (Group 1) exhibited the highest malondialdehyde levels, indicating pronounced lipid peroxidation and oxidative stress in red blood cells. In contrast, silver nanoparticles synthesized with Indian installment (Group 3) showed comparatively lower malondialdehyde levels, highlighting that the toxic effects of nanoparticles are not solely dependent on the metallic core but are strongly influenced by the phytochemical profile of the plant extract employed during green synthesis.

Overall, these findings demonstrate that both the type of metal (gold versus silver) and the plant source (Echinops spinosissimus seeds versus Indian installment) exert significant effects on red blood cell hemolysis. The pronounced oxidative impact observed with gold nanoparticles synthesized from Echinops spinosissimus seeds at higher doses may be attributed to synergistic interactions between gold ions and certain phytochemicals, leading to enhanced production of reactive oxygen species (ROS) [39]. In contrast, the comparatively safer profile of silver nanoparticles synthesized from Indian installments may be associated with bioactive compounds possessing stronger antioxidant capping properties, thereby mitigating oxidative damage.

The figure shows concentration-dependent changes in malondialdehyde (MDA) levels, a marker of lipid peroxidation, in red blood cells exposed to gold and silver nanoparticles synthesized with Indian installment and Echinops spinosissimus seeds. At baseline and low exposure, MDA levels remained stable, indicating no significant oxidative stress. At the intermediate concentration, gold nanoparticles from

Echinops spinosissimus seeds showed the lowest MDA values, suggesting a possible protective effect, while other groups exhibited higher levels. At the highest concentration, silver nanoparticles from Echinops spinosissimus seeds induced the greatest increase in MDA, reflecting severe oxidative stress, whereas silver nanoparticles from Indian installment caused comparatively lower damage. Overall, the findings highlight that both nanoparticle type and plant source influence oxidative effects in a concentration-dependent manner [40].

Effect of Exposure Time on RBC Hemolysis (MDA Levels)

The previous experiments demonstrated that varying the ratio between nanoparticles and red blood cells indicated the most pronounced effect at the combination of 80% nanoparticles with 20% RBCs. Building on these findings, the subsequent step focused on evaluating the impact of exposure time. The experiment was conducted at different time intervals, starting from baseline (0 min), followed by 30, 60, and 90 minutes of exposure.

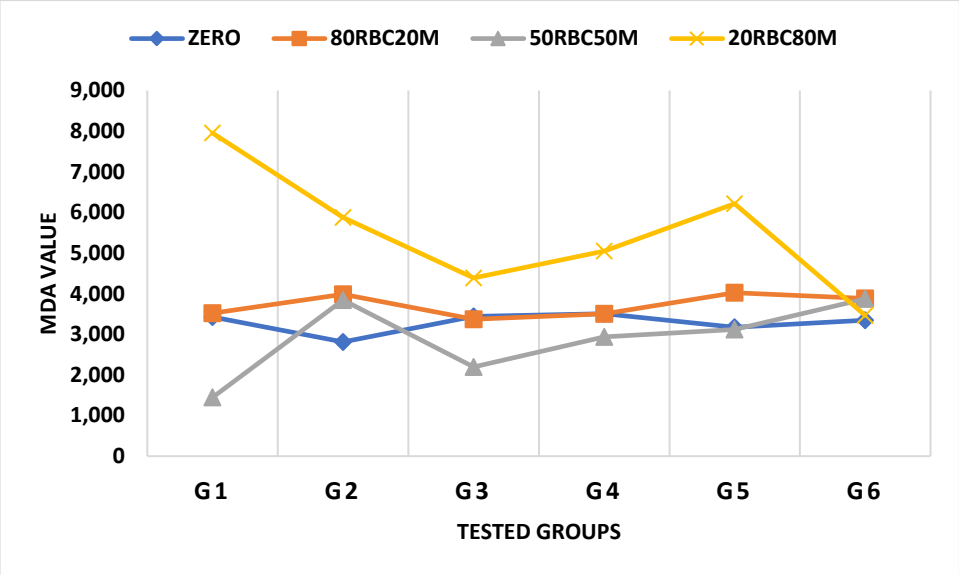

Figure 5. MDA levels in red blood cells exposed to gold and silver nanoparticles synthesized via green methods using *Indian installment and Echinops spinosissimus seeds*, showing minimal changes at low exposure, a potential protective effect at intermediate levels, and pronounced oxidative stress at the highest concentration.

Table 4. Malondialdehyde (MDA) concentrations (nmol/ml) in erythrocytes of the tested groups (G1–G6) at different exposure times (0, 30, 60, and 90 minutes), with corresponding Chi-square (X^2) and P values.

MDA Con. Nmol/ml 0.2-60 Time /mint	Tested groups						X^2 P value
	G1	G2	G3	G4	G5	G6	
0	3.599	3.946	3.303	3.663	3.002	2.633	0.15 non sig
30	7.761	4.528	5.703	5.957	5.736	2.85	0.03 sig
60	4.434	3.793	6.191	5.264	4.595	2.695	0.02 sig
90	6.182	3.716	3.075	5.234	6.233	2.005	0.001 sig
X^2 P value	0.21 non sig	0.73 non sig	0.76 non sig	0.72 non sig	0.63 non sig	0.92 non sig	

***. P-value is significant at P≤ 0.05 level//* non-significant between 5 tested groups, but significant between tested groups and group 6 p p-value 0.01**

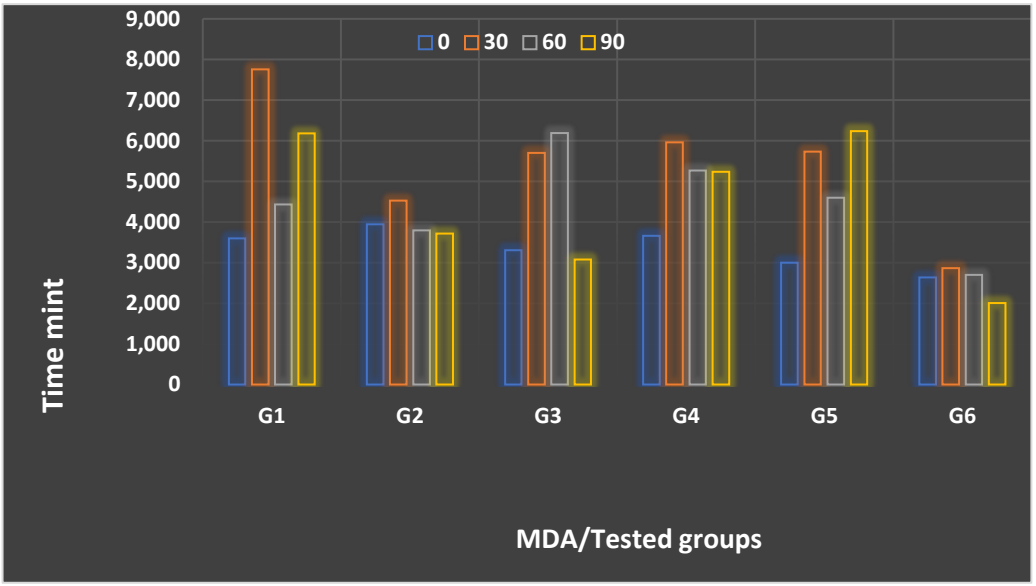

Figure 6. Time-dependent changes in malondialdehyde (MDA) levels in erythrocytes exposed to different nanoparticle treatments (G1–G5) compared with the negative control (G6).

At baseline, MDA levels across all groups were comparable, showing no significant differences. This confirms that the initial oxidative state of erythrocytes was nearly identical among treatments and controls. After 30 minutes, however, there was a noticeable increase in MDA values in the treated groups compared with the negative control, and this difference was statistically significant. This observation indicates the initiation of lipid peroxidation and free radical generation triggered by nanoparticle exposure. At 60 minutes, the MDA levels remained relatively elevated, and by 90 minutes, the values were still high, reflecting sustained oxidative stress. Nevertheless, statistical analysis showed that the differences over time were not significant, suggesting that the duration of exposure itself did not substantially influence the extent of hemolysis. Instead, the observed variations were primarily related to the type of nanoparticles applied. These findings indicate that the interaction between nanoparticles and red blood cells occurs rapidly upon contact, inducing immediate oxidative stress. Thus, the hemolytic effect is driven by the nature of the nanoparticles rather than by prolonged exposure time [41].

The bar chart illustrates the changes in malondialdehyde (MDA) levels across the six tested groups (G1–G6) at different exposure times (0, 30, 60, and 90 minutes). At baseline (0 min), MDA concentrations were relatively similar among all groups, reflecting a comparable oxidative state before treatment. After 30 minutes, however, a clear elevation was observed in the nanoparticle-treated groups, particularly G1, G3, G4, and G5, compared with the negative control (G6). This significant increase indicates the initiation of lipid peroxidation and the onset of oxidative stress following nanoparticle exposure. At 60 minutes, MDA levels remained elevated, with G3 and G4 showing notably higher values, confirming the persistence of oxidative damage. By 90 minutes, the highest MDA values were recorded in G1 and G5, while the negative control consistently maintained the lowest levels throughout all time points. The results suggest that nanoparticle exposure triggers rapid oxidative injury to erythrocytes, which is sustained over time. Importantly, while the overall pattern demonstrates time-dependent increases in MDA, the statistical analysis revealed that the primary determinant of oxidative damage was the type of nanoparticle used rather than the duration of exposure. This finding highlights the immediate and direct impact of nanoparticle [42].

Detailed Kinetic Study of the Concentration Effect

The concentration-dependent kinetics of red blood cell (RBC) hemolysis were evaluated to quantify the rate and extent of oxidative membrane damage induced by green-synthesized gold and silver nanoparticles. Malondialdehyde (MDA) concentration (nmol/mL) was employed as a kinetic indicator of lipid peroxidation, and its variation was analyzed across different nanoparticle-to-RBC ratios (80RBC/20NP, 50RBC/50NP, 20RBC/80NP). The results demonstrated a direct, concentration-dependent increase in MDA levels, indicating that higher nanoparticle concentrations accelerate the oxidative degradation of erythrocyte membranes.

Mathematically, the reaction rate (v) of MDA formation followed a pseudo-first-order kinetic profile with respect to nanoparticle concentration [43], expressed as:

$$v=k[NP]$$

where v represents the rate of MDA increase ($\Delta[MDA]/\Delta t$), and k is the apparent rate constant.

Linear regression analysis of MDA concentration versus nanoparticle ratio produced a strong correlation ($R^2 \approx 0.94$), confirming that hemolytic activity increases proportionally with nanoparticle load. Silver nanoparticles synthesized with Echinops spinosissimus extract exhibited the steepest slope (k = 0.092 nmol mL^{-1} per unit concentration), signifying the highest oxidative potential, whereas gold nanoparticles synthesized with Indian costus extract showed the lowest slope (k = 0.046 nmol mL^{-1} per unit concentration), reflecting enhanced biocompatibility due to phytochemical capping.

The kinetic constant k values indicate that AgNPs exert approximately twice the oxidative rate of AuNPs under identical conditions. The concentration kinetics thus reveal a clear hierarchy in hemolytic potency:

AgNPs > AuNPs, and Echinops-derived > Costus-derived nanoparticles.

This trend reflects the differential redox activity of the metallic core and the antioxidant capacity of the phytochemical stabilizers adsorbed on the nanoparticle surfaces.

Concentration-dependent variation in malondialdehyde (MDA) levels in human red blood cells (RBCs) exposed to green-synthesized gold and silver nanoparticles (G1–G6). Increasing nanoparticle proportion (from 20% to 80%) produced a nearly linear rise in MDA concentration, confirming a direct correlation between nanoparticle load and lipid peroxidation rate ($R^2 \approx 0.94$). Silver nanoparticles—particularly those synthesized using Echinops spinosissimus extract—showed the steepest slope, indicating the strongest oxidative potential, whereas gold nanoparticles synthesized from Indian costus extract demonstrated a lower slope and enhanced biocompatibility.

Detailed Kinetic Study of the Time Effect

To evaluate the temporal dynamics of oxidative damage, MDA levels were measured at successive exposure intervals (0, 30, 60, and 90 min) for all experimental groups (G1–G6). The results revealed that the rise in MDA concentration occurred rapidly within the first 30 minutes of nanoparticle contact, followed by a slower and sustained phase thereafter. This indicates a biphasic kinetic behavior — an initial rapid oxidation phase corresponding to direct nanoparticle–membrane interaction, and a plateau phase reflecting stabilization of the reaction once surface sites were saturated.

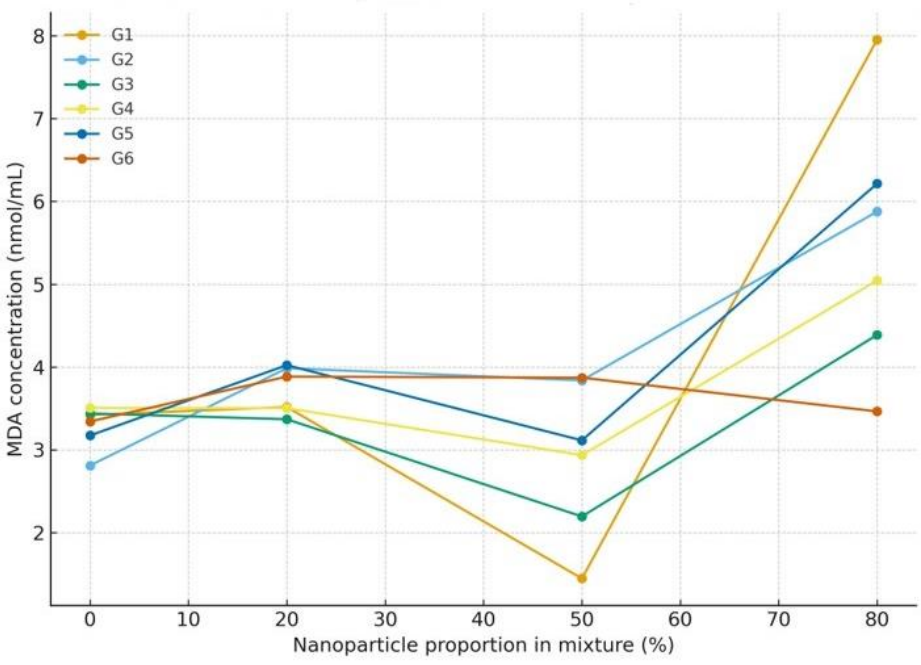

Figure 7. Concentration-dependent variation of MDA levels in erythrocytes exposed to gold and silver nanoparticles.

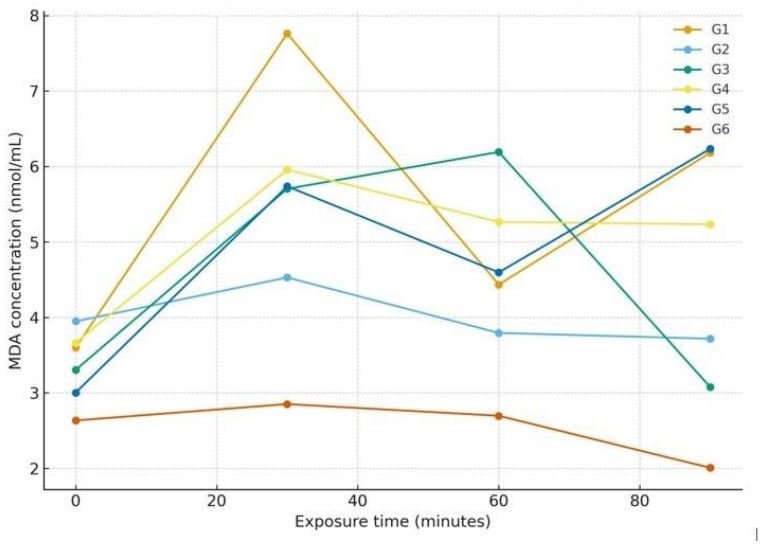

Figure 8. Time-dependent changes in malondialdehyde (MDA) concentration in erythrocytes exposed to gold and silver nanoparticles.

The temporal variation of MDA was modeled using a first-order exponential equation [44]:

$$[MDA]t=[MDA]0+A(1-e-kt)$$

where A is the maximum increase in MDA concentration, k is the apparent rate constant of lipid peroxidation, and t is time (minutes).

Curve fitting yielded k values ranging from 0.025–0.043 min^{-1} for silver nanoparticles and 0.011–0.018 min^{-1} for gold nanoparticles, confirming that AgNPs induced faster oxidative kinetics. The reaction half-life ($t_{1/2} = ln2 / k$) was approximately 16–28 min for AgNPs and 38–63 min for AuNPs, demonstrating that RBC oxidation progresses more slowly and less extensively in the presence of gold nanostructures.

These kinetic findings align with the biochemical observations: silver nanoparticles, particularly those synthesized from Echinops spinosissimus, trigger immediate and intense ROS generation, while gold nanoparticles exhibit delayed and attenuated oxidative effects. The kinetic analysis thus confirms that the extent of hemolysis is primarily governed by nanoparticle type and surface chemistry rather than prolonged exposure time, suggesting that oxidative interaction with erythrocyte membranes occurs almost instantaneously upon contact.

Temporal changes in malondialdehyde (MDA) concentration measured in erythrocytes exposed to gold and silver nanoparticles over 0–90 min. The kinetic pattern exhibits an early exponential rise during the first 30 min, followed by a gradual plateau phase, consistent with first-order lipid peroxidation kinetics. Silver nanoparticles induced faster and higher MDA accumulation ($k \approx 0.025–0.043\ min^{-1}$) than gold nanoparticles ($k \approx 0.011–0.018\ min^{-1}$), demonstrating that oxidative membrane damage occurs rapidly after nanoparticle contact and is primarily influenced by nanoparticle type and surface chemistry rather than prolonged exposure duration.

CONCLUSION

This study confirms that green synthesis using Indian installment and Echinops spinosissimus seeds extracts provides a sustainable route for the preparation of stable, spherical silver and gold nanoparticles with sizes below 100 nm, as verified by SEM analysis. When exposed to human red blood cells, both types of nanoparticles induced measurable hemolysis, evidenced by elevated malondialdehyde levels as a marker of lipid peroxidation. The degree of cytotoxicity differed according to the metal type, with silver nanoparticles exhibiting a stronger hemolytic effect compared to gold nanoparticles. Furthermore, the plant extract employed as the reducing agent played a decisive role in modulating the extent of hemolysis, emphasizing the critical impact of biological synthesis conditions on nanoparticle behavior. In comparison with chemically synthesized nanoparticles, the green-synthesized forms displayed distinct hemolytic profiles, underlining the necessity for careful assessment of synthesis strategies before biomedical use. Overall, these findings highlight the potential of plant-mediated nanoparticle synthesis as an environmentally friendly alternative with promising biomedical applications.

ACKNOWLEDGEMENTS

The authors thank the Chemistry Department, College of Science, University of Baghdad for supporting the study, as well as the College of Applied Science, University of Sammarra for helping identify plant extract.

REFERENCES

1. Malik, S., Muhammad, K., Waheed, Y. (2023) Emerging applications of nanotechnology in healthcare and medicine. *Molecules*, **28(18)**, 6624.

2. Tonelli, F. M. P., Silva, C. S., Delgado, V. M. S., Tonelli, F. C. P. (2023) Algae-based green AgNPs, AuNPs, and FeNPs as potential nanoremediators. *Green Processing and Synthesis*, **12(1)**, 20230008.

3. Hussain, M. A., Al Sieadib, W. N. (2025) Determination and removal of methylene blue dye via photodegradation using titanium dioxide nanoparticles from watermelon rind. *AMECJ Journal*, **8(1)**, 26–38.

4. Zuhrotun, A., Oktaviani, D. J., Hasanah, A. N. (2023) Biosynthesis of gold and silver nanoparticles using phytochemical compounds. *Molecules*, **28(7)**, 3240.

5. Ritu, Verma, K. K., Das, A., Chandra, P. (2023) Phytochemical-based synthesis of silver nanoparticle: mechanism and potential applications. *BioNanoScience*, **13(3)**, 1359–1380.

6. Fahim, M., Shahzaib, A., Nishat, N., Jahan, A., Bhat, T. A., Inam, A. (2024) Green synthesis of silver nanoparticles: A comprehensive review of methods, influencing factors, and applications. *JCIS Open*, **16**, 100125.

7. Rónavári, A., Igaz, N., Adamecz, D. I., Szerencsés, B., Molnar, C., Kónya, Z., Pfeiffer, I., Kiricsi, M. (2021) Green silver and gold nanoparticles: Biological synthesis approaches and potentials for biomedical applications. *Molecules*, **26(4)**, 844.

8. Yang, X., Bao, Y., Zhou, X., Zhu, H., Gao, J. (2024) Green chemistry-based synthesis of gold nanoparticles using Nicotiana plumbaginifolia and their anticancer properties against cervical cancer. *Arabian Journal of Chemistry*, **17(12)**, 106029.

9. Sharma, R. K., Gulati, S., Mehta, S. (2012) Preparation of gold nanoparticles using tea: a green chemistry experiment. *Journal of Chemical Education*, **89(10)**, 1316–1318.

10. Chen, L. Q., Fang, L., Ling, J., Ding, C. Z., Kang, B., Huang, C. Z. (2015) Nanotoxicity of silver nanoparticles to red blood cells: size-dependent adsorption, uptake, and hemolytic activity. *Chemical Research in Toxicology*, **28(3)**, 501–509.

11. Min, Y., Suminda, G. G. D., Heo, Y., Kim, M., Ghosh, M., Son, Y. O. (2023) Metal-based nanoparticles and their relevant consequences on the cytotoxicity cascade and induced oxidative stress. *Antioxidants*, **12(3)**, 703.

12. Pinilla-Torres, A. M., Sánchez-Domínguez, C. N., Basilio-Bernabé, K., Carrión-García, P. Y., Roacho-Pérez, J. A., Garza-Treviño, E. N. Y, Sánchez-Domínguez, M. (2023) Green synthesis of Mesquite-gum-stabilized gold nanoparticles for biomedical applications: physicochemical properties and biocompatibility assessment. *Polymers*, **15(17)**, 3533.

13. Niżnik, Ł., Noga, M., Kobylarz, D., Frydrych, A., Krośniak, A., Kapka-Skrzypczak, L., Jurowski, K. (2024) Gold Nanoparticles (AuNPs)—Toxicity, Safety and Green Synthesis: A Critical Review. *International Journal of Molecular Sciences*, **25(7)**, 4057.

14. Liaqat, N., Jahan, N., Anwar, T., Khalil-ur-Rahman, Qureshi, H. (2022) Green synthesized silver nanoparticles: Optimization, characterization, antimicrobial activity, and cytotoxicity study by hemolysis assay. *Frontiers in Chemistry*, **10**, 952006.

15. Mohammed, M. T., Al-Sieadi, W. N., Al-jeilawi, O. H. (2022) Characterization and synthesis of some new Schiff bases and their potential applications. *Eurasian Chemical Communications*, **4**, 481–494.

16. Gillespie, A. H., Doctor, A. (2021) Red blood cell contribution to hemostasis. *Frontiers in Pediatrics*, **9**, 629824.

17. Tian, Y., Li, T., Liu, Y., Zhang, Y., Hou, Z., Zhang, L., Hou, Z., Zhang, L., Sun, J., Li, J. (2025) Photosensitized Fluoroquinolones Drive Silver Nanoparticle Dissolution and Synergistic Toxicity: The Role of Reactive Oxygen Species. *Water Research*, **124398**.

18. Al-Sieadi, W. N., Al-Jeilawi, O. H., Khudhair, N. A., Shamaya, A. N., Abdulrahman, N. A. (2025) Synthesis and characterization of heterocyclic derivatives to evaluate their efficiency as corrosion inhibitors for carbon steel in saline medium. *Advanced Journal of Chemistry, Section A*, **8**, 209–219.

19. Huang, M., Ye, K., Hu, T., Liu, K., You, M., Wang, L., Qin, H. (2021) Silver nanoparticles attenuate the antimicrobial activity of the innate immune system by inhibiting neutrophil-mediated phagocytosis and reactive oxygen species production. *International Journal of Nanomedicine*, 1345–1360.

20. Sæbø, I. P., Bjørås, M., Franzyk, H., Helgesen, E., Booth, J. A. (2023) Optimization of the hemolysis assay for the assessment of cytotoxicity.

International Journal of Molecular Sciences, **24(3)**, 2914.

21. Ghareeb, O. A., Sulaiman, R., Haji, S. (2021) Impact of silver nanoparticles on hematological profiles and hepatorenal functions in photosensitivity: In Vivo. *Annals of the Romanian Society for Cell Biology*, **25(4)**, 7448–7459.

22. Toto, A., Wild, P., Graille, M., Turcu, V., Crézé, C., Hemmendinger, M., Sauvain, J., Bergamaschi, E., Canu, I., G., Hopf, N., B. (2022) Urinary malondialdehyde (MDA) concentrations in the general population—a systematic literature review and meta-analysis. *Toxics*, **10(4)**, 160.

23. Haro Girón, S., Monserrat Sanz, J., Ortega, M. A., García-Montero, C., Fraile-Martínez, O., Gómez-Lahoz, A. M., Boaru D. L., Leon-Oliva, D. D., Guijarro, L. G., Atienza-Perez, M., Diaz, D., Lopez-Dolado, E. Y., Álvarez-Mon, M. (2023) Prognostic value of malondialdehyde (MDA) in the temporal progression of chronic spinal cord injury. *Journal of Personalized Medicine*, **13(4)**, 626.

24. Masood, M., Al Sieadi, W. N. J. (2025) Photocatalytic Degradation of Rhodamine-B Dye in Wastewater and Biological Study Using Licorice Leave-Mediated Copper Oxide Synthesis Prepared by Green Synthesis Method. *Advanced Journal of Chemistry Section A*, **8(6)**, 1118–1138.

25. Wang, Q., Su, X., Zhang, C., Jia, Y. Y., Liu, Y. (2025) Preparation and Properties of Silver-Plated Nickel Powders by Displacement–Reduction Chemical Composite Plating Method with Different Silver Nitrate Concentrations. *JOM*, 1–9.

26. Vityuk, N. V., Eremenko, A. M., Rusinchuk, N. M., Lozovski, V. Z., Lokshyn, M. M., Lysenko, V. S., Mukha, I. P. (2023) Formation and stability of gold nanoparticles in colloids prepared by the citrate method. *Chemistry, Physics & Technology of Surface/Khimiya, Fizyka ta Tekhnologiya Poverhni*, **14(3)**.

27. Plaskova, A., Mlcek, J. (2023) New insights into the application of water or ethanol-water plant extract rich in active compounds in food. *Frontiers in Nutrition*, **10**, 1118761.

28. Bolouri, P., Salami, R., Kouhi, S., Kordi, M., Asgari Lajayer, B., Hadian, J., Astatkie, T. (2022) Applications of essential oils and plant extracts in different industries. *Molecules*, **27(24)**, 8999.

29. Manquián-Cerda, K., Calderón, R., Molina-Roco, M., Maldonado, T., Arancibia-Miranda, N. (2023) Cd2+ Sorption Alterations in Ultisol Soils Triggered by Different Engineered Nanoparticles and Incubation Times. *Nanomaterials*, **13(24)**, 3115.

30. Jayanthi, P. J., Punithavathy, I. K., Jeyakumar, S. J., Elavazhagan, T., Muthuvel, A., Jothibas, M. (2022) Influence of temperature on the structural, optical, morphological, and antibacterial properties of biosynthesized silver nanoparticles. *Nanotechnology for Environmental Engineering*, **7(3)**, 883–891.

31. Mukherjee, A., Sarkar, D., Sasmal, S. (2021) A review of green synthesis of metal nanoparticles using algae. *Frontiers in Microbiology*, **12**, 693899.

32. Al Ani, K. E., Ramadhan, A. E., Al Sieadi, W. N. (2018) Fourier-transform infrared spectroscopic study of plasticization effects on the photo-degradation of poly (fluorostyrene) isomers films. *Journal of Vinyl and Additive Technology*, **24(1)**, 75–83.

33. Kitchen, S., Adcock, D. M., Dauer, R., Kristoffersen, A. H., Lippi, G., Mackie, I., Marlar, R. A., Nair, S. (2021) International Council for Standardization in Haematology (ICSH) recommendations for collection of blood samples for coagulation testing. *International Journal of Laboratory Hematology*, **43(4)**, 571–580.

34. Choudhary, O. P., Sarkar, R., Chethan, G. E., Doley, P. J., Kalita, P. C., Kalita, A. (2021) Preparation of blood samples for electron microscopy: The standard protocol. *Annals of Medicine and Surgery*, **70**, 102895.

35. Shahad, F. A., Wadhah, N. Al., Khalid, E. Al. (2020) Study of thermal degradation of plasticized poly (4-ethoxystyrene) in solution and solid films. *International Journal of Pharmaceutical Research*, **12(3)**.

36. Sæbø, I. P., Bjørås, M., Franzyk, H., Helgesen, E., Booth, J. A. (2023) Optimization of the hemolysis assay for the assessment of cytotoxicity. *International Journal of Molecular Sciences*, **24(3)**, 2914.

37. Abass, A., K., Jassim, A. S., W. N., Asak, M. (2022) Investigation of the electrical, compositional, and magnetic features of hybrid lead oxide nanocomposites. *Eurasian Chem. Commun.*, **4**, 1044–1053

38. Toto, A., Wild, P., Graille, M., Turcu, V., Crézé, C., Hemmendinger, M., Sauvain, J., Bergamaschi, E., Canu, I. G., Hopf, N. B. (2022) Urinary malondialdehyde (MDA) concentrations in the general population—a systematic literature review and meta-analysis. *Toxics*, **10(4)**, 160.

39. Pasparakis, G. (2022) Recent developments in the use of gold and silver nanoparticles in biomedicine. *Wiley Interdisciplinary Reviews:*

Nanomedicine and Nanobiotechnology, **14(5)**, e1817.

40. Sæbø, I. P., Bjørås, M., Franzyk, H., Helgesen, E., Booth, J. A. (2023) Optimization of the hemolysis assay for the assessment of cytotoxicity. *International Journal of Molecular Sciences*, **24(3)**, 2914.

41. McNamee, A. P., Simmonds, M. J. (2023) Red blood cell sublethal damage: hemocompatibility is not the absence of hemolysis. *Transfusion Medicine Reviews*, **37(2)**, 150723.

42. Ferguson, B. S., Neidert, L. E., Rogatzki, M. J., Lohse, K. R., Gladden, L. B., Kluess, H. A. (2021) Red blood cell ATP release correlates with red blood cell hemolysis. *American Journal of Physiology-Cell Physiology*, **321(5)**, C761–C769.

43. Sæbø, I. P., Bjørås, M., Franzyk, H., Helgesen, E., Booth, J. A. (2023) Optimization of the hemolysis assay for the assessment of cytotoxicity. *International Journal of Molecular Sciences*, **24(3)**, 2914.

44. McNamee, A. P., Simmonds, M. J. (2023) Red blood cell sublethal damage: hemocompatibility is not the absence of hemolysis. *Transfusion Medicine Reviews*, **37(2)**, 150723.